Time-Resolved EPR Studies of Charge Recombination and Triplet-State Formation within Donor-Bridge-Acceptor Molecules Having Wire-Like Oligofluorene Bridges

ARTICLE *in* THE JOURNAL OF PHYSICAL CHEMISTRY A · APRIL 2010

Impact Factor: 2.69 · DOI: 10.1021/jp101523n · Source: PubMed

3 AUTHORS, INCLUDING:

Raanan Carmielli
Weizmann Institute of Science
44 PUBLICATIONS **881** CITATIONS

Time-Resolved EPR Studies of Charge Recombination and Triplet-State Formation within Donor−Bridge−Acceptor Molecules Having Wire-Like Oligofluorene Bridges

Tomoaki Miura, Raanan Carmieli, and Michael R. Wasielewski*

Department of Chemistry and Argonne−Northwestern Solar Energy Research (ANSER) Center, Northwestern University, Evanston, Illinois 60208-3113

Received: February 19, 2010; Revised Manuscript Received: March 22, 2010

Spin-selective charge recombination of photogenerated radical ion pairs within a series of donor−bridge−acceptor (D−B−A) molecules, where D = phenothiazine (PTZ), B = oligo(2,7-fluorenyl), and A = perylene-3,4:9,10-bis(dicarboximide) (PDI), PTZ−FL_n−PDI, where n = 1−4 (compounds **1**−**4**), is studied using time-resolved electron paramagnetic resonance (TREPR) spectroscopy in which the microwave source is either continuous-wave or pulsed. Radical ion pair TREPR spectra are observed for **3** and **4** at 90−294 K, while the neutral triplet state of PDI (^{3}*PDI) is observed at 90−294 K for **2**−**4** and at 90 K for **1**. ^{3}*PDI is produced by three mechanisms, as elucidated by its zero-field splitting parameters and spin polarization pattern. The mechanisms are spin−orbit-induced intersystem crossing (SO-ISC) in PDI aggregates, direct spin−orbit charge-transfer intersystem crossing (SOCT) from the singlet radical pair within **1**, and radical pair intersystem crossing (RP-ISC) as a result of S−T_0 mixing of the radical ion pair states in **2**−**4**. The temperature dependence of the spin−spin exchange interaction ($2J$) shows a dramatic decrease at low temperatures, indicating that the electronic coupling between the radical ions decreases due to an increase in the average fluorene−fluorene dihedral angle at low temperatures. The charge recombination rates for **3** and **4** decrease at low temperature, but that for **2** is almost temperature-independent. These results strongly suggest that the dominant mechanism of charge recombination for $n \geq 3$ is incoherent thermal hopping, which results in wire-like charge transfer.

Introduction

A molecular wire is a molecular bridge that can move charge rapidly and efficiently over many chemical bond lengths.[1−4] Such molecular bridges are an intrinsic feature of primary photosynthetic charge separation in reaction center proteins, in which rapid, stepwise electron transfer occurs between redox cofactors.[5] The need to transport charge over long distances in molecular systems for artificial photosynthesis and organic photovoltaics makes it important to understand the fundamental nature of wire-like molecular systems. There have been reported two distinct mechanisms of charge transport, which are superexchange and thermally activated hopping. The superexchange mechanism of coherent charge transport from the donor to the acceptor results from quantum mechanical mixing of the donor state with bridge states that are higher in energy and energetically well-separated from those of the donor.[6] Charge transfer occurs in a single step with a rate that decays exponentially with donor−acceptor distance (r_{DA}) that is described by the damping factor β. In contrast, hopping occurs by actual oxidation/reduction of the bridge moiety.[7] Ultimately, charge trapping occurs at the acceptor whose electron affinity is greater than that of the bridge. Charge-transport rates for the hopping mechanism are only weakly distance-dependent ($1/r_{DA}$), allowing charge to move efficiently at long distances, so that systems exhibiting this mechanism are termed "molecular wires".[1,8]

Perylene-3,4:9,10-bis(dicarboximide) (PDI) has been extensively studied as a photoredox agent in artificial photosynthetic systems[9−17] because it strongly absorbs visible light,[18] is readily reduced,[19] and has a negligible yield of direct spin−orbit-induced intersystem crossing (SO-ISC) to ^{3}*PDI.[20,21] PDI-based dyes are also capable of self-assembling into extended structures by means of $\pi-\pi$ stacking,[14−16,22−32] which can be utilized for construction of highly organized supramolecular photodriven systems. Recent reports on both covalent[33] and self-assembled[22] cofacial PDI dimers, however, have shown that such dimers give significant yields of ^{3}*PDI via formation of an excimer-like state,[34] which is not possible for PDI monomers. The effect of aggregation on photodriven charge transport in PDI-based donor−bridge−acceptor (D−B−A) systems has not been explored in detail, even though rapid ^{3}*PDI formation is detrimental to the yield of photodriven charge separation, especially in materials designed for use in organic photovoltaics.[35]

Time-resolved electron paramagnetic resonance (TREPR) spectroscopy is one of the most powerful methods to study charge recombination and triplet generation reactions because it can be used to monitor radical ion pair (RP) and triplet excited-state dynamics directly. From the TREPR spectra of spin-correlated radical pairs,[36,37] we can estimate the spin−spin exchange coupling $2J = E_S - E_T$, where E_S and E_T are energy levels of the singlet and triplet radical pairs, respectively, which directly reflects the electronic coupling between the donor and acceptor (V_{DA}).[38−42] Zero-field splitting parameters of triplet-state TREPR spectra are quite sensitive to slight delocalization of triplet excitation among the two π systems of dimer molecules.[43−46] Spin polarization patterns of TREPR spectra of triplet states are also informative with regard to the intersystem crossing mechanism by which triplet states are generated.[43,47−51]

In this paper, we report TREPR spectra of a D−B−A molecular wire system (PTZ−FL_n−PDI) consisting of a covalently linked PDI chromophoric electron acceptor, an oligo(2,7-fluorenyl) bridge (FL_n), and a phenothiazine donor (PTZ). Nanosecond transient optical absorption measurements in room-

* To whom correspondence should be addressed. E-mail: m-wasielewski@northwestern.edu.

10.1021/jp101523n
Published on Web 04/14/2010

temperature toluene[1] suggest that charge recombination in PTZ−FL$_n$−PDI, where $n > 2$, is governed largely by a thermally activated incoherent hopping mechanism, that is, wire-like electron transfer,[7,52,53] rather than a coherent superexchange mechanism.[54−58] The dominance of the hopping mechanism has been attributed to the low charge injection barrier to the FL$_n$ bridge, which has an oxidation potential that is almost independent of bridge length.[1,3,59] The formation of ^{3}*PDI following RP charge recombination has also been observed by transient optical absorption, which is attributed to the RP-ISC mechanism.

In this paper, we use TREPR to carefully examine the spin-selective charge recombination mechanism of the photogenerated RP leading to ^{3}*PDI in the PTZ−FL$_n$−PDI series, where $n = 1-4$ (**1**−**4**) in the context of the impact of self-assembly of these molecule into higher aggregates on the charge-transfer dynamics as a function of temperature.

Experimental Section

The synthesis and characterization of compounds PTZ−FL$_n$−PDI (**1**−**4**) and reference molecules PDI−FL$_n$ (**5** and **6**, $n = 1$ and 3) have been reported previously.[1]

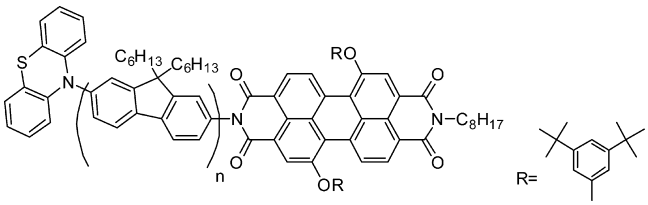

Samples (∼0.1 mM) were dissolved in toluene and loaded into 4 mm OD, 2 mm ID quartz tubes and degassed by 4−5 freeze−pump−thaw cycles on a vacuum line (10^{-4} Torr). Samples were then sealed using a hydrogen torch. All samples were prepared in freshly distilled ACS-grade toluene. For the measurement of **1**, we added about 2% polystyrene (average molecular weight of 280 000) to the toluene solution in order to form good glass at low temperature; otherwise, we could not obtain reproducible EPR spectra.[60]

The experimental setup for TREPR used here is similar to what has been described elsewhere.[50,61] A Bruker E580 X-band EPR spectrometer was used for TREPR using both continuous-wave (CW) and pulsed microwaves to detect the transient EPR signals. The temperature was controlled by an Oxford Instruments CF935 continuous flow cryostat using liquid N_2. Samples set inside of the resonator were irradiated at 532 nm (1.5−2.0 mJ/pulse, 7 ns) using the frequency-doubled output from a Nd:YAG laser (QuantaRay Lab 150).

For the TREPR experiments using CW microwaves, the kinetic traces of the transient signals were obtained using quadrature detection. For each trace, the signal acquired prior to laser excitation of the sample was subtracted from the data in both the real and imaginary channels. The signal phase was adjusted to detect the imaginary part of the transient magnetization χ'', which is presented as the EPR signal. A short time response of $Q/\pi\nu \approx 50$ ns was achieved by disabling the field modulation and using a dielectric resonator, which has a low quality factor ($Q \approx 1500$). Sweeping the magnetic field gave 2D spectra versus the time and field. Kinetic traces recorded at the off-resonance field were subtracted from the data, and final 2D spectra with microwave emission (e) or absorption (a) were obtained. The typical microwave power was ∼0.6 mW. For the measurement of the TREPR kinetics, the microwave power was reduced to avoid transient nutations.

For the pulsed TREPR measurements, a standard two-pulse electron spin−echo pulse sequence was used. A $\pi/2$ pulse with a duration of 8 ns (1 kW TWT amplifier) was applied to the overcoupled dielectric resonator ($Q \approx 200$) at a time t_d after the laser pulse. The transverse magnetization created by the $\pi/2$ pulse was refocused by a subsequent π pulse (16 ns duration) at T following the initial $\pi/2$ pulse. The echo signal, which appeared at T following the π pulse, was detected by the quadrature detector. A typical value for T was 108 ns. The phases of the signals were adjusted so that the signal appeared exclusively in either the real or imaginary channel and is presented as χ''.

Results

Femtosecond transient absorption experiments have shown that photoexcitation of **1**−**4** results in rapid formation of ^{1}*PDI followed by electron transfer from PTZ to ^{1}*PDI to give the singlet RPs, PTZ$^{+\bullet}$−FL$_n$−PDI$^{-\bullet}$ at both room temperature and at low temperature (∼200 K).[1,25] The charge-separation time constants are all shorter than the ∼4.5 ns lifetime of ^{1}*PDI,[18,34] so that the CS kinetics in **1**−**4** are too fast to be observed directly by TREPR techniques. Nanosecond transient optical absorption spectroscopy of **1**−**4** at room temperature has revealed that charge recombination (CR) occurs in tens to hundreds of nanoseconds, which results in the formation of ^{3}*PDI.[1]

Figure 1A shows TREPR spectra for **1** in 90 K. The spectra are all assigned to ^{3}*PDI based on the total width of the zero-field splitting pattern $2D \approx 80$ mT.[22,61] At 90 K and early times, the spin polarization of all six canonical lines of the spectra is (e,e,e,a,a,a) (from low field to high field). However, at later times, the spin polarization pattern changes dramatically to (e,a,e,a,e,a). It has been observed that irradiation of a solution of **1** at temperatures above 150 K, where toluene is considered to be in a soft crystalline phase, results in the formation of a stable photoproduct that makes the (e,a,e,a,e,a) polarized signal much stronger. Data is only presented at 90 K, where the spectra for **1** are reproducible.

Figure 1B−D shows the time- and temperature-dependent TREPR spectra for **2**−**4**, respectively. All spectra presented here are assigned to ^{3}*PDI, which is also accompanied by the relatively narrow spin-correlated radical pair (SCRP) signal at the center field.[36,37,61] At temperatures that are lower than the melting point of toluene, the ^{3}*PDI spectra at early times exhibit the (e,e,e,a,a,a) polarization pattern regardless of the bridge length. However, the polarization pattern changes into (a,e,e,a,a,e) at later times. Interestingly, not only does the polarization pattern change with time, but so does the value of the zero-field splitting parameter D, which becomes larger at later times regardless of the bridge length. The temperature dependence of spectral features in the 90−150 K range is weak. The kinetic profiles for **3** at 90 K for two magnetic fields are shown in Figure 2. The RP signal at the center field appears with the instrument response time and decays in hundreds of nanoseconds. The highest-field band of the ^{3}*PDI signal shows the time-dependent change in polarization from a to e. The time constant for this polarization change is similar to that of the RP signal decay, whereas the resulting emissive signal at late times decays very slowly.

At 180 K, which is slightly above the melting point of toluene, the ^{3}*PDI signal for **2**−**4** only has the (a,e,e,a,a,e) polarization pattern, which is also observed at late times at lower temperatures. The spectra at early times, however, show weaker

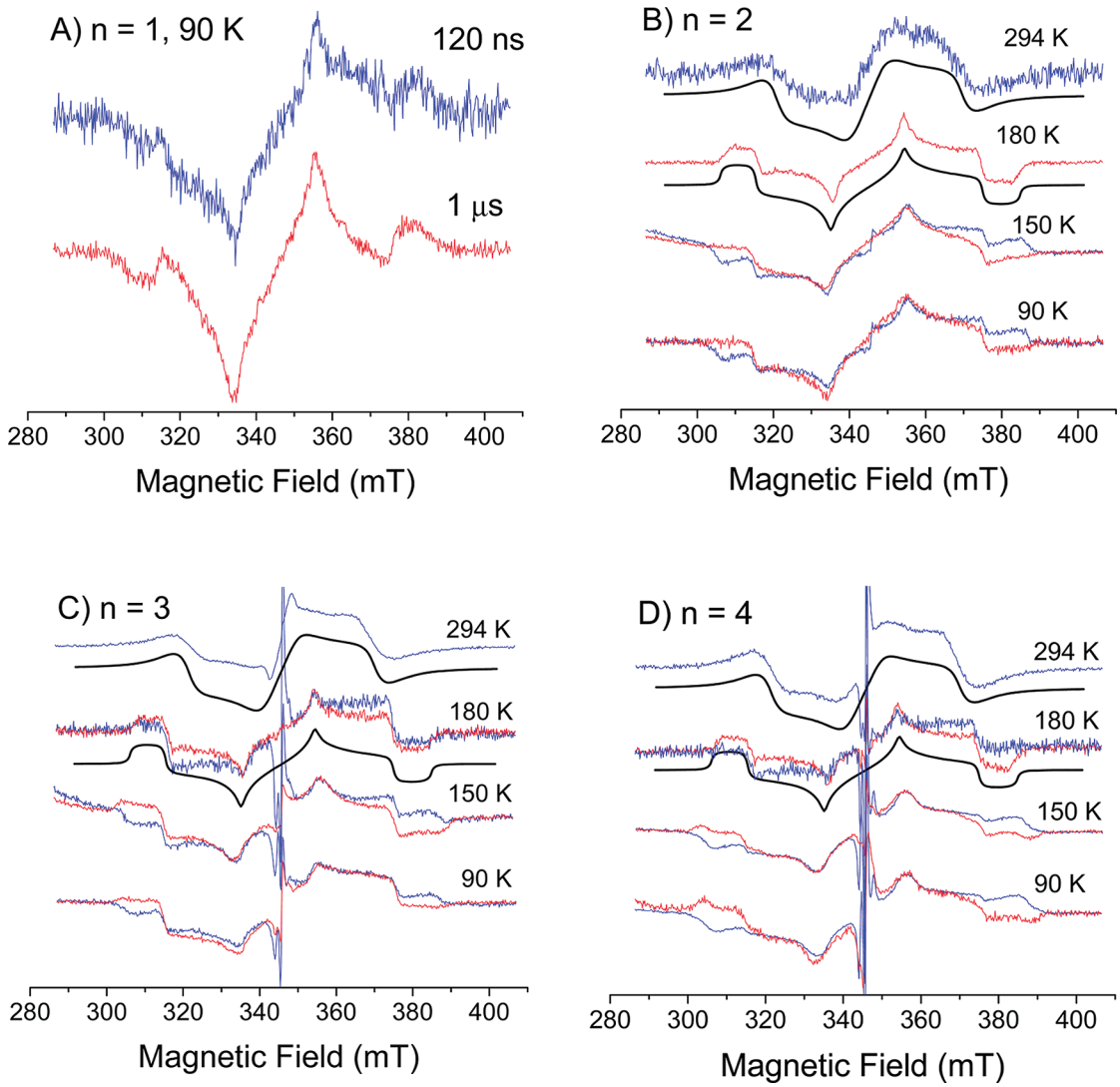

Figure 1. TREPR spectra for **1**−**4** (A−D) at the indicated temperatures. Blue and red trace lines indicate spectra at early (∼100 ns) and late times (0.5−1 μs), respectively. Black smooth lines indicate simulations with parameters shown in Table 1.

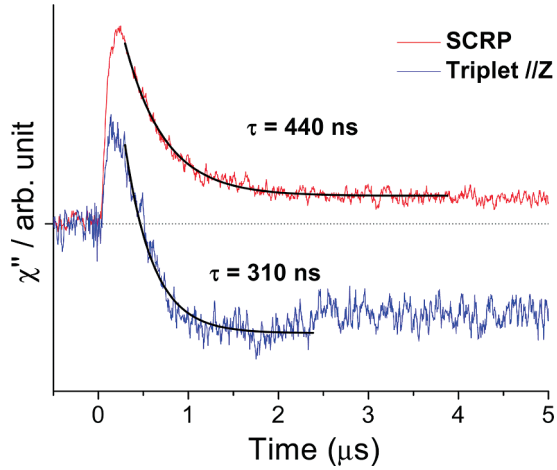

Figure 2. Kinetics of the TREPR signal of **3** at 90 K. The blue trace is the time profile of the triplet EPR signal at the highest magnetic field canonical point, while the red trace corresponds to the magnetic field at the peak of the spin-correlated radical pair spectrum.

outermost bands and stronger shoulder signals relative to the peak signal, indicating a slight contribution of e and a polarization on lowest- and highest-field canonical lines, respectively. The total line width of the ^{3}*PDI spectra is smaller than that observed at 90 K at late times, although their polarization patterns are identical.

We observe well-resolved ^{3}*PDI spectra with good signal-to-noise for **3** and **4** even at room temperature. The triplet spectrum for **4** accompanies a narrow SCRP spectrum at the center field. In the case of **3**, the ^{3}*PDI spectrum accompanies a structureless signal having e/a polarization with splitting of 5 mT. The remainder of the spectrum is identical to that for **4**, indicating that the broad e/a signal for **3** results from a SCRP. As for the broad signal due to ^{3}*PDI, the (a,e,e,a,a,e) polarization pattern at the canonical turning points is less clear due to the broadening. For **2**, we have observed a weak ^{3}*PDI signal but no RP signal at room temperature. The spectral shape of the ^{3}*PDI signal is almost identical to those of **3** and **4**.

Pulsed EPR measurements have been applied to **1** and **3** at 90 K. The integrated spin−echo intensity is plotted as a function of the external magnetic field with fixed t_d and T (field-swept, echo-detected (FSED) spectra) and shown in Figure 3. We assume that the FSED spectra are more quantitative than transient CW spectra for triplet states in frozen solvents, especially when using a dielectric resonator, which has a much higher fill factor than conventional EPR resonators. This results from the fact that saturation effects on spectra due to long longitudinal relaxation times (T_1) and the relatively large

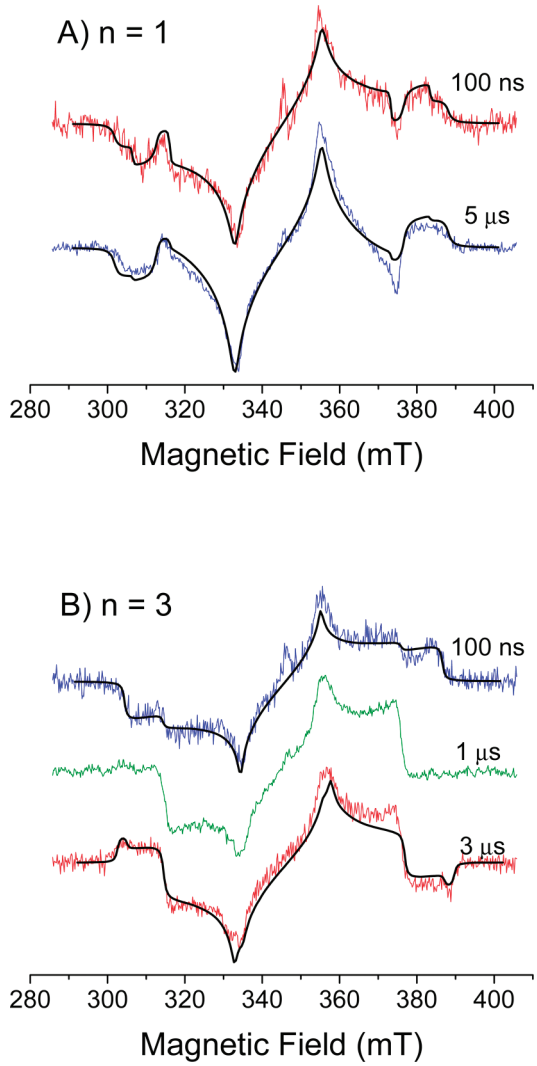

Figure 3. Field-swept echo-detected spectra for (A) **1** and (B) **3** at 90 K at the indicated delay times after the laser pulse. Black lines are simulations by the method described in the text with the parameters in Table 1.

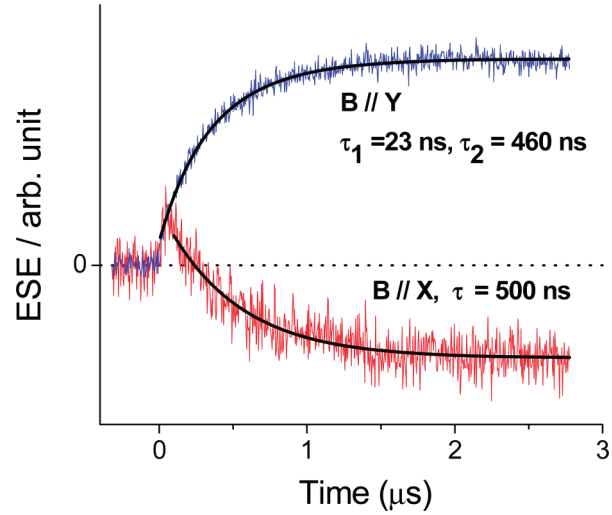

Figure 4. Kinetics of the TREPR signal of **1** at 90 K obtained by delay time dependence of the spin−echo signal. The blue line corresponds to higher field line of the two innermost canonical points ($B||Y$ assuming $D > 0$ and $E < 0$) whereas the red one is obtained at the lower field line of the middle canonical points ($B||X$).

microwave fields (B_1) used to obtain transient CW EPR spectra with good S/N ratio cannot be ignored. The spectra are assigned entirely to ^{3}*PDI with no signal at center field from the RP, which is most likely due to the short RP lifetime relative to the length of the microwave pulse sequence used to obtain the spectra. We assign the weak absorptive, sharp signal at the center field to a stable radical created by slight photodegradation of the sample, which has been confirmed by measurements without laser excitation that follow a period of signal acquisition with laser excitation. The t_d dependence of the triplet polarization pattern of **1** and **3** is qualitatively the same as that observed by transient CW EPR, namely, from (e,e,e,a,a,a) to (e,a,e,a,e,a) for **1** and from (e,e,e,a,a,a) to (a,e,e,a,a,e) for **3**. For **3**, the total width of the spectrum as determined by $2D$ changes as a function of time. While a similar change for **1** is likely, its outermost canonical turning point is not clear at late times, which makes it difficult to assess the total change in $2D$.

The t_d dependence of the integrated echo intensity for **1** at the innermost and second innermost canonical magnetic field positions is presented in Figure 4. The signal for $B||Y$ shows a biexponential rise of 23 and 460 ns, whereas the signal for $B||X$ shows a fast rise of the absorptive signal at the earliest time, which then changes its phase to an emissive signal at later times. The time change of the polarization occurs on a similar time scale to the slower rising component of the biexponential $B||Y$ signal.

Reference molecules **5** and **6**, which lack the PTZ donor, also show triplet EPR signals at low temperatures (Figure 5). The polarization pattern is (e,e,e,a,a,a) at all observation times. The relative intensity of the innermost canonical turning points is larger for **6** than that of **5**. The polarization pattern for **6** is very similar to that of the early time spectrum for **3**, although the total splitting for **6** is slightly larger. The spectral shape does not change at 180 K for both **5** and **6**, which do not give any EPR signals at room temperature. In fact, no SCRP signals are observed for **5** and **6** at any temperature.

SCRP spectra for **3** and **4** recorded with a smaller magnetic field step size are summarized in Figure 6A and B, respectively. We have observed weak SCRP signals for **2** at temperatures lower than the solvent melting point, which, however, are so weak and broad that we cannot separate them from the more intense triplet signals. As for **3** and **4** at room temperature, the background signal due to the triplet signal at the center field is approximately fit by a third-order polynomial function and can be subtracted from the RP signal. In the remaining cases, the triplet background signal is assumed to be linear with that magnetic field, and each baseline triplet signal is subtracted from the RP EPR spectrum. The spectral shape for each molecule does not show significant changes at temperatures below the solvent melting point but drastically sharpens above the melting point and becomes broader again at room temperature. The dependence of the spectral shape on the bridge length is also evident and tends to be broader for the shorter bridges at the same temperature.

Discussion

Spin Polarization Patterns. We have observed three different spin polarization patterns for **1**−**4**, namely, (e,e,e,a,a,a), (e,a,e,a,e,a), and (a,e,e,a,a,e). These polarization patterns should give us information about precursor states of the triplet states. The fact that the same (e,e,e,a,a,a) polarization pattern has been observed for **1**−**4**, and even for reference molecules **5** and **6** without PTZ, suggests that this polarization pattern has nothing to do with charge recombination of the radical pair because no

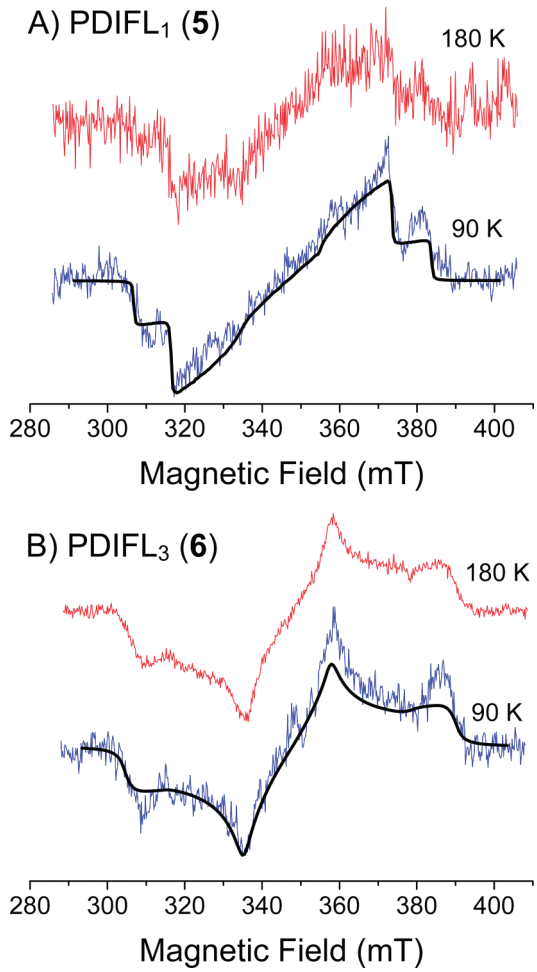

Figure 5. Field-swept echo-detected spectra for reference molecules (A) **5** and (B) **6** at the indicated temperatures. The black lines are simulations with parameters in Table 1.

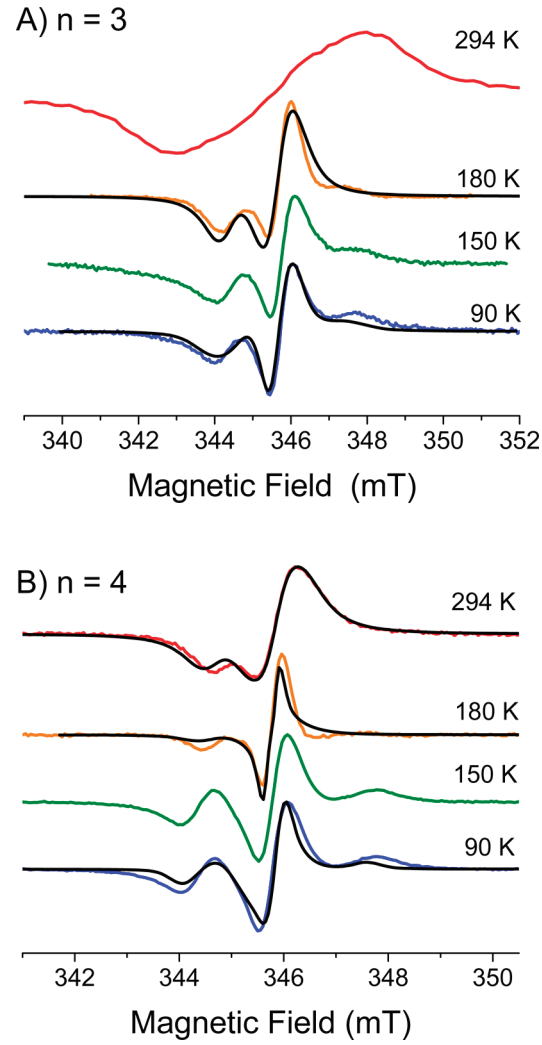

Figure 6. Spin-correlated radical pair spectra of (A) **3** and (B) **4** at the indicated temperatures obtained by time-resolved CW EPR with small field steps. The triplet background signal is subtracted by the method described in the text. Black lines are simulations by the method described in the Discussion section.

electron transfer is observed for **5** and **6**.[1] Furthermore, it is well-known that direct SO-ISC from ^{1}*PDI to ^{3}*PDI is negligible for PDI monomers.[20,21] Temperature dependence studies of the UV−vis absorption spectra for this particular system have revealed that these PDI−FL$_n$−PTZ molecules aggregate cofacially at low temperatures.[25] Recently, Veldman et al.[33] have reported on a covalently linked, cofacial PDI dimer in which the triplet state is generated from an excimer-like state via a proposed charge-transfer intermediate state. Using the same covalently linked PDI dimers as well as PDI-based DNA conjugates, we have observed that cofacial PDI dimers in frozen solutions give triplet EPR signals with the same polarization pattern.[22] From these findings, we conclude that the triplet state with the (e,e,e,a,a,a) polarization pattern is generated from the excimer-like state of aggregated PDI. The aggregation number and its polydisperity are unclear from the TREPR spectra, but it has been observed that the photophysical properties of cofacial PDI trimers are similar to those of the dimers.[34]

If spin−orbit-induced anisotropic ISC results in overpopulation of the zero-field T_X and T_Y sublevels and $D > 0$ and $E < 0$, we expect (e,e,e,a,a,a) polarization. The positive D value is expected because the lowest triplet excited state is a $\pi-\pi^*$ excited state.[48,49] We have simulated the FSED spectra of **5** and **6** at 90 K and $t_d = 500$ ns by the conventional simulation method for spin-polarized triplet EPR spectra (Figure 5)[62,63] and have obtained the fitting parameters summarized in Table 1. The spectra are reproduced well by the simulation with overpopulation on the zero-field T_X and T_Y sublevels. This suggests that SO-ISC takes place so that the geometry of orbital angular momentum change is in the $Y-Z$ and $X-Z$ planes of PDI.[64,65] It is reasonable to assume that the Z-axis is the out-of-plane axis, as is typical of $\pi-\pi^*$ triplets of aromatic molecules, which leaves the X and Y axes in the plane of ^{3}*PDI.[66,67] The dimer triplet state is generated from a singlet state that has a certain amount of CT character,[33] which can be described as PDI$^{\delta-}$PDI$^{\delta+}$. The polarization pattern indicates that charge recombination from the PDI$^{\delta-}$ LUMO to the PDI$^{\delta+}$ HOMO occurs with an angular momentum change in the $Y-Z$ and $X-Z$ planes. More population on T_X for **5** than **6** could be related to a different molecular structure of the dimer aggregates, indicating that the length of the FL$_n$ bridge affects the dimer structure.

The (e,a,e,a,e,a) polarization pattern is observed only for **1**. This polarization pattern can be explained by overpopulation of the zero-field T_Y sublevel. According to earlier studies of an analogous PDI−Ph$_n$−PTZ system in which Ph$_n$ is a oligomeric p-phenylene bridge, a similar polarization pattern was observed only when $n = 1$.[61] SCRP spectra are not observed for both **1** and PDI−Ph$_1$−PTZ; in addition, neither molecule shows a magnetic field effect on its triplet yield. This indicates that the $2J$ coupling of the RPs in these systems is very large. In that

TABLE 1: Triplet-State Parameters Obtained from the Spectral Simulations

sample	temperature (K)	polarization	population ratio	D (mT)	$\|E\|$ (mT)
1	90 K	dimer SOC (data for **5**)	$P_X/P_Y = 1{:}0.46$	38.5	6.2
		RP-SOC	$P_X/P_Y = 0{:}1$	43.1	6.9
3	90 K	dimer SOC	$P_X/P_Y = 0.67{:}1$	41.1	6.8
		RP-ISC	$P_{T0} = 1$	43.5	6.3
	180 K	RP-ISC	$P_{T0} = 1$	39.3	6.7
	294 K	RP-ISC	$P_{T0} = 1$	28.8	6.6
6	90 K (∼180 K)	dimer SOC	$P_X/P_Y = 0.47{:}1$	42.7	6.7

case, coherent interconversion between the singlet and triplet manifolds by hyperfine and Δg interactions, that is, RP-ISC, is inefficient because the singlet−triplet energy gap ($2J$) is large. Instead, the large electronic coupling of the singlet RP can induce direct ISC to the triplet excited state by a SO interaction within the radical pair, a process that we have termed SOCT.[50,51,68,69]

T_Y overpopulation is expected if direct charge recombination by SOCT takes place with an angular momentum change in the $X-Z$ plane. The ground-state energy-minimized structure for this particular system shows that the D−B and B−A dihedral angles are close to 90° and the N atom of PTZ is basically tetrahedral.[1,3] In this case, the Z-axis of PDI is likely to be in the same plane with the p_z orbital of the N and S atoms of PTZ, which have most of the charge (spin) density. If the principal x-axis is parallel to the N−N axis of PDI, then electron transfer between the two π systems results in an angular momentum change in the $X-Z$ plane, which results in overpopulation of T_Y.

Our previous studies of the PDI−Ph_n−PTZ system[61] have pointed out that it is possible that SOCT contributes to triplet formation for $n > 1$, but we did not take into account the possibility that aggregation might also play a role in the overall ISC process. The results that we present here suggest that SO-ISC in the aggregated D−B−A molecules most likely contributes to the overall triplet yield even if $2J$ is too small to permit direct SOCT from the singlet radical pairs. The (a,e,e,a,a,e) polarization pattern cannot be explained by selective sublevel population in the zero-field basis set as in previous cases. If $D > 0$ and the high field T_0 sublevel is overpopulated, the polarization pattern becomes (a,e,e,a,a,e), as observed for **2**−**4**. This polarization pattern is characteristic of RP-ISC followed by charge recombination from the T_0 sublevel of the triplet RP to the neutral triplet of the D−B−A molecule.[43,47] This mechanism is strongly suggested from the fact that the phase change of the outermost lines of the triplet spectra takes place on a similar time scale as the decay of the SCRP signal (Figure 2).

Triplet-State Formation Kinetics. At temperatures below the melting point of the solvent, the initial spin-polarized triplet signal from aggregates of **2**−**4** evolves into the triplet signal characteristic of the RP-ISC-derived triplet. It is clear that generation of the triplet state in the aggregates is very fast (<50 ns) based on the fast rise of the signal (Figure 2). According to time-resolved fluorescence lifetime studies of cofacial PDI dimers,[34] the emission from the excimer-like state has a lifetime of ∼20 ns in room-temperature toluene. Thus, it is likely that SO-ISC of the cofacial PDI aggregates also takes place in <50 ns.

We have clearly observed slow kinetics (approximately a few hundred nanoseconds) for the formation of RP-ISC-derived ^{3}*PDI, which match the kinetics for the SCRP signal decay in **2**−**4** (Figures 1 and 2). The large difference in formation rates for the two ^{3}*PDI signals makes it relatively easy to observe both of them. The FSED spectrum for **3** at early times was simulated by the conventional method, and the parameters are shown in Table 1. The population ratios are not very different from those of **6**. At late times, the spectra are dominated by RP-ISC polarization. This spectrum, however, cannot be perfectly simulated assuming T_0 population by RP-ISC alone. The data are better simulated by mixing a fraction of the simulated early time spectrum with the late time spectrum. This is understandable because there should be some fraction of the aggregate-derived signal remaining even at late times considering its long T_1. The dipolar interaction for the RP-ISC-derived spectral component ($D = 43.5$ mT) is larger than that for the aggregate-derived component ($D = 41.1$ mT). It is well-known that D decreases when the triplet state is shared among two or more molecules resulting from a CT interaction.[43−46] Thus, the RP-ISC triplet signal with larger D is considered to result from more monomer-like D−B−A molecules, namely, the two triplet generation pathways mainly result from inhomogeneity of aggregation.

Interestingly, the D value of the triplet state observed for the reference molecule **6** ($D = 42.7$ mT) is smaller than that for RP-ISC component of **3** but larger than that of the aggregate spectrum. Furthermore, the dipolar splitting for **6** is independent of the observation time, unlike those of the D−B−A systems. These phenomena are qualitatively well-explained assuming the inhomogeneity of aggregation and the kinetics of the triplet formation processes as follows. Following photoirradiation of aggregated D−B−A molecules, the singlet state is quenched by either formation of the excimer-like state or electron transfer from the donor to the acceptor. The efficiency of excimer-like state formation, which eventually results in SO-ISC triplet formation, is expected to be higher for shorter PDI−PDI cofacial distances. On the other hand, electron transfer from PTZ to ^{1}*PDI within the same molecule is not strongly influenced by the aggregation because the singlet energy and the RP energy level are both affected by the aggregation so that the free energy for electron transfer remains approximately constant, as we have observed previously.[1,3] In the D−B−A systems described here, SO-ISC in the tightly aggregated PDI molecules leads to ^{3}*PDI at early times, whereas in the loosely aggregated D−B−A molecules, electron transfer is kinetically competitive. Such loose aggregates do not give a triplet signal at early times and yield a triplet signal with a larger D value only at later times due to RP-ISC followed by slow charge recombination. On the other hand, without the PTZ donor, loosely aggregated D−B−A molecules are also expected to contribute to a SO-ISC-derived triplet signal because electron transfer does not take place. In this case, we do not expect a delayed signal from the loosely aggregated D−B−A molecules. Thus, we observe a D value for **6** that is larger than that for the aggregated component of the D−B−A triplet at all observation times. The larger D value for the RP-ISC component of **3** relative to that for **6** is simply explained by contributions from nonaggregated molecules, which never give a SO-ISC-derived triplet state.

A similar description for the triplet-state generation kinetics of **1** can be made. The time dependence of the FSED spectra indicates that the SO-ISC-derived triplet signal of the aggregates is followed by the slow rise of SOCT-derived triplet signal. A rise time of ~400 ns is observed by the t_d dependence of the integrated echo signal (Figure 4) and is likely determined by SOCT-induced charge recombination of the singlet RP to the triplet state. The FSED spectra at early and late times cannot be simulated by a single ISC mechanism. The spectra at late times are simulated by a superposition of the dominant SOCT component (T_Y overpopulated) and the aggregate SO-ISC component taken from the simulated spectrum of **5**. The spectrum at early times is nicely simulated by increasing the amount of the SO-ISC mechanism due to aggregation. However, separation of the aggregate SO-ISC component from the subsequent SOCT component is not as good as that achieved for **3**. Consequently, the population ratio and D value for the aggregation SO-ISC component of **1** have some uncertainty. The SOCT component gives a larger D value of 43.1 mT than that for **5** (D = 38.5 mT). It is very likely that monomer-like molecules give RPs and aggregated D−B−A molecules give excimer-like states, as is the case for the longer bridge lengths.

Raising the temperature slightly above the melting point of the solvent results in a dramatic decrease of the ^{3}*PDI signal resulting from SO-ISC in the aggregates of **2**−**4**, whereas we can still observe a significant signal from aggregates of reference molecules **5** and **6**. The spectra for **2**−**4** at late times are all well-simulated by a single RP-ISC-derived triplet state with T_0 population. The temperature dependence of the UV−vis spectra indicates that some aggregation occurs in this temperature region.[25] It is likely that the electron-transfer rate is accelerated by greater solvent mobility near the melting point,[70] which allows the RP-ISC pathway for **2**−**4** to dominate at higher temperatures.

At room temperature, we do not observe any ^{3}*PDI signal resulting from SO-ISC in the aggregates in the triplet spectra for **2**−**4**; therefore, the spectrum is due entirely to the RP-ISC-derived triplet. This observation is further supported by the fact that we cannot observe any EPR or nanosecond transient absorption signal for a triplet state in **5** and **6** at room temperature. This is expected because the UV−vis spectra of **5** and **6** show no evidence of aggregation at room temperature.[1,25]

To conclude, the aggregation state of the PDI-based D−B−A molecules determines which triplet formation pathway dominates, ISC via the excimer-like ^{1}*PDI$_n$ state or electron transfer between D and A. The kinetic competition between these two pathways depends on optimizing the rates of electron transfer. We have observed efficient electron transfer in some self-assembled PDI-based systems with negligible triplet formation.[14,71] In these systems, charge transfer is sufficiently fast compared to formation of the excimer-like state, or the energy level of the radical pair is lower than the excimer-like state, so that charge separation from the excimer takes place.

Triplet-State Dynamics in the Liquid Phase. It is noteworthy that we have observed the triplet EPR spectra of PDI in **1**−**4** even at room temperature. In the case of most organic compounds, the dipolar interaction of their triplet states is averaged out by fast rotation of the molecules, and their EPR signal with fine structure is rarely observed at room temperature.[72−74] Observation of the triplet spectra for **3** and **4** at room temperature indicates that the rotation of these large D−B−A molecules is slow. The decay kinetics of the triplet signal at room temperature is very fast (~ 50 ns) compared to that at 180 K (a few hundreds of nanoseconds), which indicates that T_1 is shorter at room temperature. The broad line width of the signals at the canonical turning points indicates that T_2 is also very short at room temperature. As a consequence, the rotational correlation time at room temperature is very slow but still faster than that at 180 K, where toluene is a viscous liquid.

The zero-field splitting parameters for the RP-ISC-derived triplet spectra obtained by simulation are temperature-dependent, as shown in Table 1. These parameters for **3** give a smaller D value at higher temperatures but give almost the same E values even at room temperature. This effect is understood as an averaging of the dipolar interaction due to anisotropic molecular rotation. It has been reported for planar molecules, such as unsubstituted porphyrins, that in-plane rotation takes place at relatively low temperatures, and out-of-plane rotation is observed only at higher temperatures.[73] In this case, E is easily averaged to 0, namely, energy levels of T_X and T_Y are averaged out, and an axially symmetric zero-field splitting is observed by increasing the temperature above the melting point of the solvent. Further increases in temperature induce out-of-plane rotation, which results in only a single line. In our case, PDI is attached to a large bridge−acceptor moiety and in-plane rotation is highly restricted, possibly even at room temperature, giving rise to averaging of only D.

The weak signal of **2** is most likely due to the slow triplet formation rate and the much faster triplet relaxation rate. This is supported by the kinetics of **2** at room temperature, whose rise and decay times are 100 and 300 ns, respectively. The rise time of 100 ns is close to the decay time of the triplet signal for **3** and **4**, which is likely to be determined by T_1 considering the fast triplet formation rate. The 300 ns decay time is close to the RP lifetime observed by nanosecond transient absorption spectroscopy at room temperature. Thus, the triplet signal of **2** at room temperature shows inverted kinetics, and the signal intensity is very small. It is surprising that the molecular motion of ^{3}*PDI at room temperature seems to be independent of bridge length for n = 2−4, considering their identical spectral shape (i.e., D, E, and T_2) and very similar decay rate (T_1). The long alkyl chains attached to the FL$_n$ bridge might inhibit the rotation of the entire D−B−A molecule as well.

Regarding reference molecules **5** and **6**, the total splitting width at 180 K is similar to that at 90 K. The spitting is larger than that for the RP-ISC-derived triplet for **3** (D = 39.2 mT) at the same temperature. This fact indicates that motional averaging of D is inefficient for PDI aggregates at 180 K. The π-stacking interaction within the aggregate likely inhibits the out-of-plane rotational motion of the PDI moiety.

Radical Pair Spectral Simulations. We have simulated the RP TREPR spectra for n = 2−4 at several temperatures. The method used here is the conventional stick simulation with a Lorentzian line width based on SCRP theory.[36,37] At temperatures lower than the toluene melting point, broader spectra than those obtained at 180 K are observed. Thus, all of the anisotropic interactions are taken into account. The parameters for PTZ$^{+\bullet}$, including the g tensor and hyperfine tensor of the N atom, are taken from literature values for chemically oxidized, unsubstituted PTZ as [g_{xx}, g_{yy}, g_{zz}] = [2.0072, 2.0060, 2.0024] and [a_{Nxx}, a_{Nyy}, a_{Nzz}] = [0.175, 0.175, 1.745] (mT), respectively.[75] It is very likely that the z-axes for the g and the hyperfine tensors are perpendicular to the π system of PTZ$^{+\bullet}$; the z-axes for each tensor are considered to be identical. The anisotropy of PDI$^{-\bullet}$ is obtained from the W-band, field-swept echo-detected spectrum of chemically reduced, unsubstituted 1,7-bis(3,5-diphenoxy)PDI. The anisotropy at W-band mainly comes from the g tensor which is [g_{xx}, g_{yy}, g_{zz}] = [2.0037, 2.0031, 2.0017]. Since the in-plane

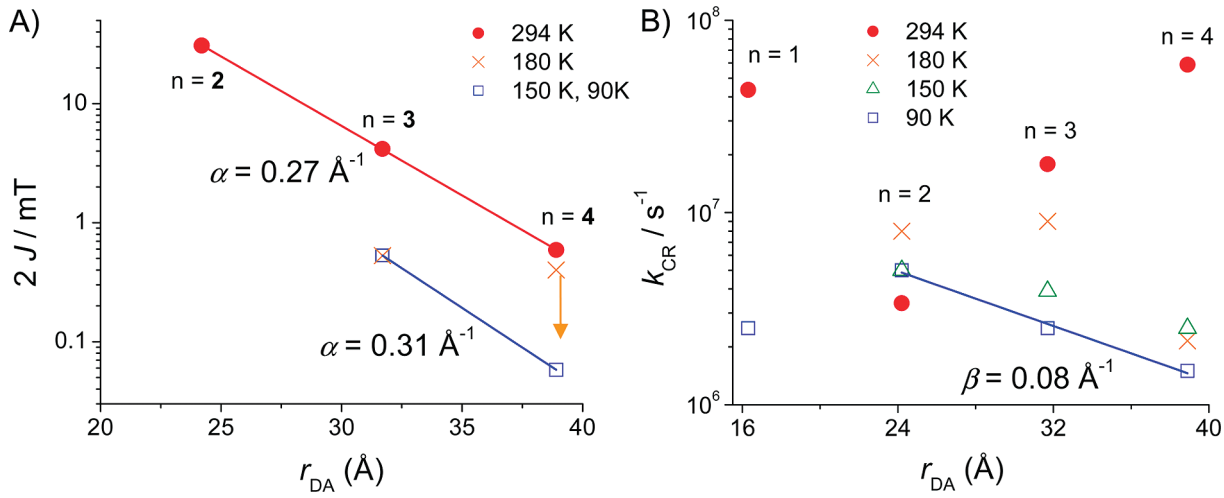

Figure 7. (A) Log plot of 2*J* obtained by simulation of the SCRP spectra (90−180 K). The value of 2*J* for **4** at 180 K is shown as an upper limit. (B) Log plot of the charge recombination rate obtained by EPR kinetics (90−180 K). All of the room-temperature results are obtained by nanosecond transient absorption and magnetic field effect measurements described in ref 1. The values of α and *β* are slopes obtained by the linear fit of the distance dependence of 2*J* and k_{CR}, respectively.

anisotropy (difference between the *x* and *y* principal values) for both radicals is relatively small, the anisotropy is assumed to be axially symmetric, and averaged in-plane components are used. It turns out that this approximation does not affect the simulated spectra for simulation at X-band. The hyperfine couplings of other nuclei are assumed to be isotropic.

Both the spin−spin exchange interaction (2*J*) and the dipolar interaction within the RP are taken into account in the simulations. The relative orientation of the dipolar axis with regard to the molecular axis is fixed, and orientation inhomogeneity is assumed to be part of the line width. The distance between the donor and acceptor is taken from AM1 calculations,[1] and the angle between the dipolar axis and the magnetic field is averaged over $0-\pi/2$. The effect of spin-selective recombination on the spectral shape is ignored for simplicity. According to the theory of Till and Hore,[76] spin-selective recombination distorts the spectra on the time scale of (k_S-k_T), where k_S and k_T are the charge recombination rates from the singlet and triplet manifolds, respectively. From the fact that the time dependence of the spectra is not very obvious for all molecules and temperatures, k_S and k_T are likely comparable. Besides, the spectra at late times cannot be clearly observed due to their weak signals and the relatively large triplet background signal, making it more difficult to extract recombination rates from the spectral simulations. As a consequence, we have simulated spectra at an early time (∼100 ns), where the effects of RP recombination would be less significant but line broadening due to the rise of the magnetization is gone.

At both 180 K and room temperature, anisotropy of the hyperfine and Zeeman interactions is ignored for simplicity. This treatment seems to be valid at room temperature but may not be valid at 180 K, where rotational motion of the RP is considered to be somewhat slower. However, we have no way to take into account this slow rotation for a stick simulation, and the motion is likely to be fast at 180 K considering the drastic reduction in total line width over the melting point. The fact that triplet spectra are observed for **3** and **4** at 180 K and room temperature, rotation of the entire D−B−A molecule is likely to be very slow even at room temperature. Similar to the discussion above, it is very difficult to treat such slow motions. For simplicity, we have taken into account the dipolar interaction in fluid solution as well as that in the frozen solvent.

Comparisons of the simulations for **3** at 90 and 180 K and for **4** at 90, 180 K, and room temperature with the experimental RP spectra are presented in Figure 6. The 2*J* values are plotted in Figure 7A as a function of r_{DA}. We have not simulated the spectra for **3** at room temperature and for **2** in frozen solvent because the spectra lack sufficient structure for an accurate simulation. Such broad e/a spectra are obtained in the case where line widths are large and the spin−spin interactions are small.[77] In this small splitting limit, one can never obtain an accurate 2*J* or *D* value from the spectral simulation. Unfortunately, the spectra for **4** at 180 K and room temperature are in this limit, and we have obtained only the maximum value of 2*J* from the simulation ($2J \leq 0.4$ mT for both cases). This maximum value at room temperature is consistent with the 2*J* value obtained by magnetic field effects on the triplet yield.[1]

In frozen toluene, the 2*J* values are determined rather accurately thanks to well-defined broadening mechanisms, which are the anisotropy of the hyperfine and Zeeman interactions. It turns out that the relative orientation of the dipolar axis and the *g* tensor is not a very sensitive parameter in the case of **3** due to large 2*J* value and the additional line width needed for the simulation. The simulation of the RP spectra for **4** is rather sensitive to the orientation parameters. The relative angles between the dipolar axis and the *z*-axis of the *g* tensor are $\theta_{DZ}(PTZ) \approx 30°$ and $\theta_{DZ}(PDI) \approx 30°$ for $PTZ^{+\bullet}$ and $PDI^{-\bullet}$, respectively. Unlike linear bridges such as oligo(*p*-phenylenes), oligofluorene bridges have uncertainty in the molecular structure due to the 2,7-bond angle of the fluorene. Thus, a θ_{DZ} of 30° seems to be possible. However, we cannot determine the absolute structure of the RP due to the small anisotropy, the overlap of the radical signals at X-band, and the large additional line width. This line width could be due to an inhomogeneous distribution of RP structures because more line width is needed for **3** than **4**.

Charge Recombination Dynamics and Electronic Coupling. The decay kinetics of the SCRP signal at low temperature is on the order of 10^6 s^{-1}. The decay of the SCRP signal is determined by the sum of the charge recombination rate and $1/T_1$. At low temperature, T_1 is usually much longer than 1 μs, and charge recombination is likely to be the dominant component that determines the decay kinetics.[78] Thus, the decay rates can be safely used to estimate the lower limit of the charge recombination rate. Charge recombination rates (k_{CR}) obtained

from exponential fitting of the decay kinetics are plotted as a function of the donor−acceptor distance (r_{DA}) in Figure 7B. The room-temperature data are taken from previously reported results using nanosecond transient absorption measurements.[1] The decay time constants of the SCRP signal at room temperature for **3** and **4** are consistent with the transient absorption data considering the time resolution of the spectrometer, which is comparable to k_{CR}. As for **2** at 180 K, we cannot observe the SCRP signal but can observe the RP-ISC-derived triplet signal. The rise time of the *Z* component of the triplet signal is plotted instead of the decay time of the SCRP. Likewise, the rise time of the SOCT-derived triplet signal of **1** at 90 K is plotted as the charge recombination rate of the RP. We have observed a clear temperature dependence of k_{CR} for **3** and **4**, but that for **2** is weaker. The drastic decrease of k_{CR} for **3** and **4** at low temperatures supports the idea that thermally activated charge hopping determines the charge recombination rate. On the other hand, the insensitivity of k_{CR} for **2** to temperature indicates that the dominant recombination mechanism for **2** is coherent superexchange, which is known to have a weaker temperature dependence.[7]

As mentioned above, the 2*J* values obtained from the SCRP simulation are plotted in Figure 7A. In this case as well, the 2*J* values at room temperature are obtained from nanosecond transient absorption detected magnetic field effects,[1] which is a more suitable method for determining 2*J* when it is much larger than the hyperfine interaction. The 2*J* values for **2**−**4** are 1 order of magnitude smaller at low temperatures than those at room temperature. The 2*J* coupling of radical pairs is strongly related to the electronic coupling interaction between the donor and acceptor as given by

$$2J = \Delta E_S - \Delta E_T = \left[\sum_n \frac{|\langle\psi_{RP}|V_{RP-n}|\psi_n\rangle|^2}{E_{RP} - E_n - \lambda}\right]_S - \left[\sum_n \frac{|\langle\psi_{RP}|V_{RP-n}|\psi_n\rangle|^2}{E_{RP} - E_n - \lambda}\right]_T \quad (1)$$

where the indicated matrix elements couple the singlet and triplet RP states to states *n*, E_{RP} and E_n are energies of these states, respectively, and λ is the total nuclear reorganization energy of the charge recombination reaction.[38−41] Since the solvent reorganization energy, λ_S, of toluene is negligible, the total reorganization energy is relatively small (∼0.6 eV),[1,3] and the dominant factor for the temperature dependence of 2*J* is considered to be the total electronic coupling matrix element. It has been suggested from studies of some D−B−A systems that the dihedral rotational motions of the bridge−bridge single-bond junctions increase the effective electronic coupling.[4,79] This rotational motion is greatly slowed or eliminated at low temperatures, resulting in a preference for large dihedral angles in the distribution of rotamers, which most likely decouples the π systems of the bridge segments giving rise to smaller overall effective coupling.

The value of V_{DA} is known to decay exponentially with r_{DA}, indicating that the distance dependence of 2*J* coupling is also expressed by the equation

$$2J(r_{DA}) = 2J_0 \exp[-\alpha(r_{DA} - r_0)] \quad (2)$$

where α is a constant and $2J_0$ is the value of the spin−spin exchange interaction at r_0, the minimum RP separation.[1,3,56] At room temperature, a linear fit of the log(2*J*) plot gives a decay factor of $\alpha = 0.27$ Å^{-1}. At 90 K, a similar α value of ∼0.3 Å^{-1} has been obtained, albeit using only two data points. The weak, broad, and nearly structureless nature of the SCRP signal for **2** at 90 K indicates that 2*J* is larger than the effective hyperfine coupling. It is likely that that 2*J* value is a few mT, which is consistent with the linear fit for two data points. These decay factors reflect the distance dependence of the superexchange component of the charge recombination reaction.[1,3]

As it has been noted above, the distance dependence of k_{CR} at room temperature does not show an exponential decay, indicating that the incoherent hopping mechanism may be operative. However, at 90 K, we can fit the data by the exponential function

$$k_{CR}(r_{DA}) = k_{CR0} \exp(-\beta_{CR} r_{DA}) \quad (3)$$

and have obtained $\beta_{CR} = 0.08$ Å^{-1}. This small β_{CR} value supports the idea that the hopping mechanism still dominates at low temperature. The β_{CR} value is much smaller than α, so that there is a residual contribution from the superexchange mechanism at 90 K. The problem inherent in this analysis and that of the previous Ph_n bridges is that the distance dependence of k_{CR} reflects the total decay rate, which is a mixture of charge recombination to the singlet ground state and to the triplet state. In such cases, the RP-ISC process could affect the CR kinetics. A detailed analysis of EPR and MFE data to separate the singlet and triplet manifold of RP recombination for Ph_n bridges has been presented[80] and will be presented for the fluorenyl bridge system in a future publication.

Conclusion

By using TREPR techniques, we have observed the lowest triplet states of PDI−FL_n−PTZ and have clearly separated the three triplet-state formation pathways. SO-ISC with T_X and T_Y overpopulation is observed for PDI aggregates at low temperatures. Direct SOCT from the singlet radical pair to the triplet state is observed only for $n = 1$, which shows T_Y overpopulation. RP-ISC followed by charge recombination gives triplet states with the high field T_0 state overpopulated in the case of $n = 2-4$.

Radical pair TREPR spectra are observed for $n = 2-4$. The spectral simulations give 2*J* values that are about 10 times smaller at low temperatures than those at room temperature, indicating that the two radicals in the RP have a much smaller effective electronic coupling at low temperature due to elimination of bridge−bridge torsional motions. The CR rates for **3** and **4** are dramatically reduced at low temperatures, whereas that for **2** is almost temperature-independent, indicating that the dominant mechanism at room temperature is thermal hopping for **3** and **4** and superexchange for **2**. The CR rate at 90 K shows a small exponential decay factor of $\beta = 0.08$ Å^{-1}, which implies a residual contribution from the hopping mechanism.

Acknowledgment. We thank Dr. Randall H. Goldsmith for the synthesis of PTZ−FL_n−PDI molecules. This work was supported by the Chemical Sciences, Geosciences, and Biosciences Division, Office of Basic Energy Sciences, DOE under Grant No. DE-FG02-99ER14999.

References and Notes

(1) Goldsmith, R. H.; Sinks, L. E.; Kelley, R. F.; Betzen, L. J.; Liu, W. H.; Weiss, E. A.; Ratner, M. A.; Wasielewski, M. R. *Proc. Natl. Acad. Sci. U.S.A.* **2005**, *102*, 3540–3545.

(2) Ratner, M. A.; Jortner, J. In *Molecular Electronics*; Jortner, J. R., Mark, Ed.; Blackwell: Oxford, U.K., 1997; pp 5−72.
(3) Weiss, E. A.; Ahrens, M. J.; Sinks, L. E.; Gusev, A. V.; Ratner, M. A.; Wasielewski, M. R. *J. Am. Chem. Soc.* **2004**, *126*, 5577–5584.
(4) Weiss, E. A.; Tauber, M. J.; Kelley, R. F.; Ahrens, M. J.; Ratner, M. A.; Wasielewski, M. R. *J. Am. Chem. Soc.* **2005**, *127*, 11842–11850.
(5) Parson, W. W. *Photosynth. Res.* **2003**, *76*, 81–92.
(6) Jortner, J.; Bixon, M.; Langenbacher, T.; Michel-Beyerle, M. E. *Proc. Natl. Acad. Sci. U.S.A.* **1998**, *95*, 12759–12765.
(7) Berlin, Y. A.; Burin, A. L.; Ratner, M. A. *Chem. Phys.* **2002**, *275*, 61–74.
(8) Weiss, E. A.; Wasielewski, M. R.; Ratner, M. A. *Top. Curr. Chem.* **2005**, *257*, 103–133.
(9) Wasielewski, M. R. *J. Org. Chem.* **2006**, *71*, 5051–5066.
(10) Xu, W.; Chen, H.; Wang, Y.; Zhao, C.; Li, X.; Wang, S.; Weng, Y. *ChemPhysChem* **2008**, *9*, 1409–1415.
(11) Shibano, Y.; Umeyama, T.; Matano, Y.; Tkachenko, N. V.; Lemmetyinen, H.; Imahori, H. *Org. Lett.* **2006**, *8*, 4425–4428.
(12) Ozcan, O.; Yukruk, F.; Akkaya, E. U.; Uner, D. *Top. Catal.* **2007**, *44*, 523–528.
(13) Wasielewski, M. R. *Chem. Rev.* **1992**, *92*, 435–461.
(14) Rybtchinski, B.; Sinks, L. E.; Wasielewski, M. R. *J. Phys. Chem. A* **2004**, *108*, 7497–7505.
(15) Rybtchinski, B.; Sinks, L. E.; Wasielewski, M. R. *J. Am. Chem. Soc.* **2004**, *126*, 12268–12269.
(16) van der Boom, T.; Hayes, R. T.; Zhao, Y. Y.; Bushard, P. J.; Weiss, E. A.; Wasielewski, M. R. *J. Am. Chem. Soc.* **2002**, *124*, 9582–9590.
(17) Gust, D.; Moore, T. A.; Moore, A. L. *Acc. Chem. Res.* **1993**, *26*, 198–205.
(18) Ahrens, M. J.; Sinks, L. E.; Rybtchinski, B.; Liu, W. H.; Jones, B. A.; Giaimo, J. M.; Gusev, A. V.; Goshe, A. J.; Tiede, D. M.; Wasielewski, M. R. *J. Am. Chem. Soc.* **2004**, *126*, 8284–8294.
(19) Gosztola, D.; Niemczyk, M. P.; Svec, W.; Lukas, A. S.; Wasielewski, M. R. *J. Phys. Chem. A* **2000**, *104*, 6545–6551.
(20) Ford, W. E.; Kamat, P. V. *J. Phys. Chem.* **1987**, *91*, 6373–6380.
(21) Kircher, T.; Lohmannsroben, H. G. *Phys. Chem. Chem. Phys.* **1999**, *1*, 3987–3992.
(22) Carmieli, R.; Zeidan, T. A.; Kelley, R. F.; Mi, Q.; Lewis, F. D.; Wasielewski, M. R. *J. Phys. Chem. A* **2009**, *113*, 4691–4700.
(23) Chen, S.-G.; Branz, H. M.; Eaton, S. S.; Taylor, P. C.; Cormier, R. A.; Gregg, B. A. *J. Phys. Chem. B* **2004**, *108*, 17329–17336.
(24) Chen, Y. L.; Kong, Y.; Wang, Y. F.; Ma, P.; Bao, M.; Li, X. Y. *J. Colloid Interface Sci.* **2009**, *330*, 421–427.
(25) Goldsmith, R. H.; DeLeon, O.; Wilson, T. M.; Finkelstein-Shapiro, D.; Ratner, M. A.; Wasielewski, M. R. *J. Phys. Chem. A* **2008**, *112*, 4410–4414.
(26) Kaiser, T. E.; Wang, H.; Stepanenko, V.; Wuerthner, F. *Angew. Chem., Int. Ed.* **2007**, *46*, 5541–5544.
(27) Tang, T. J.; Qu, J. Q.; Mullen, K.; Webber, S. E. *Langmuir* **2006**, *22*, 26–28.
(28) Wang, W.; Han, J. J.; Wang, L. Q.; Li, L. S.; Shaw, W. J.; Li, A. D. Q. *Nano Lett.* **2003**, *3*, 455–458.
(29) Wang, W.; Li, L. S.; Helms, G.; Zhou, H. H.; Li, A. D. Q. *J. Am. Chem. Soc.* **2003**, *125*, 1120–1121.
(30) Wang, Y. F.; Chen, Y. L.; Li, R. J.; Wang, S. Q.; Su, W.; Ma, P.; Wasielewski, M. R.; Li, X. Y.; Jiang, J. Z. *Langmuir* **2007**, *23*, 5836–5842.
(31) Weitzel, C. R.; Everett, T. A.; Higgins, D. A. *Langmuir* **2009**, *25*, 1188–1195.
(32) Yan, P.; Chowdhury, A.; Holman, M. W.; Adams, D. M. *J. Phys. Chem. B* **2005**, *109*, 724–730.
(33) Veldman, D.; Chopin, S. M. A.; Meskers, S. C. J.; Groeneveld, M. M.; Williams, R. M.; Janssen, R. A. J. *J. Phys. Chem. A* **2008**, *112*, 5846–5857.
(34) Giaimo, J. M.; Lockard, J. V.; Sinks, L. E.; Scott, A. M.; Wilson, T. M.; Wasielewski, M. R. *J. Phys. Chem. A* **2008**, *112*, 2322–2330.
(35) Howard, I. A.; Laquai, F.; Keivanidis, P. E.; Friend, R. H.; Greenham, N. C. *J. Phys. Chem. C* **2009**, *113*, 21225–21232.
(36) Buckley, C. D.; Hunter, D. A.; Hore, P. J.; McLauchlan, K. A. *Chem. Phys. Lett.* **1987**, *135*, 307–312.
(37) Closs, G. L.; Forbes, M. D. E.; Norris, J. R. *J. Phys. Chem.* **1987**, *91*, 3592–3599.
(38) Anderson, P. W. *Phys. Rev.* **1959**, *115*, 2–13.
(39) Kobori, Y.; Sekiguchi, S.; Akiyama, K.; Tero-Kubota, S. *J. Phys. Chem. A* **1999**, *103*, 5416–5424.
(40) Kramers, H. A. *Physica* **1934**, *1*, 182–192.
(41) Weiss, E. A.; Ratner, M. A.; Wasielewski, M. R. *J. Phys. Chem. A* **2003**, *107*, 3639–3647.
(42) Kobori, Y.; Yamauchi, S.; Akiyama, K.; Tero-Kubota, S.; Imahori, H.; Fukuzumi, S.; Norris, J. R., Jr. *Proc. Natl. Acad. Sci. U.S.A.* **2005**, *102*, 10017–10022.
(43) Budil, D. E.; Thurnauer, M. C. *Biochim. Biophys. Acta* **1991**, *1057*, 1–41.
(44) Ishii, K.; Yamauchi, S.; Ohba, Y.; Iwaizumi, M.; Uchiyama, I.; Hirota, N.; Maruyama, K.; Osuka, A. *J. Phys. Chem.* **1994**, *98*, 9431–9436.
(45) Norris, J. R.; Budil, D. E.; Gast, P.; Chang, C. H.; Elkabbani, O.; Schiffer, M. *Proc. Natl. Acad. Sci. U.S.A.* **1989**, *86*, 4335–4339.
(46) Saiful, I. S. M.; Heinze, P.; Ohba, Y.; Yamauchi, S.; Yamamoto, M.; Tohda, Y.; Tani, K. *Mol. Phys.* **2006**, *104*, 1535–1542.
(47) Hoff, A. J.; Deisenhofer, J. *Phys. Rep.* **1997**, *287*, 2–247.
(48) Hutchison, C. A.; Mangum, B. W. *J. Chem. Phys.* **1958**, *29*, 952–953.
(49) Levanon, H.; Norris, J. R. *Chem. Rev.* **1978**, *78*, 185–198.
(50) Dance, Z. E. X.; Mickley, S. M.; Wilson, T. M.; Ricks, A. B.; Scott, A. M.; Ratner, M. A.; Wasielewski, M. R. *J. Phys. Chem. A* **2008**, *112*, 4194–4201.
(51) van Willigen, H.; Jones, G., II; Farahat, M. S. *J. Phys. Chem.* **1996**, *100*, 3312–3316.
(52) Davis, W. B.; Svec, W. A.; Ratner, M. A.; Wasielewski, M. R. *Nature* **1998**, *396*, 60–63.
(53) Davis, W. B.; Wasielewski, M. R.; Ratner, M. A.; Mujica, V.; Nitzan, A. *J. Phys. Chem.* **1997**, *101*, 6158–6164.
(54) Closs, G. L.; Miller, J. R. *Science* **1988**, *240*, 440–447.
(55) Closs, G. L.; Piotrowiak, P.; MacInnis, J. M.; Fleming, G. R. *J. Am. Chem. Soc.* **1988**, *110*, 2652–2653.
(56) McConnell, H. M. *J. Chem. Phys.* **1961**, *35*, 508–515.
(57) Paddon-Row, M. N.; Oliver, A. M.; Warman, J. M.; Smit, K. J.; Dehaas, M. P.; Oevering, H.; Verhoeven, J. W. *J. Phys. Chem.* **1988**, *92*, 6958–6962.
(58) Roest, M. R.; Oliver, A. M.; Paddon-Row, M. N.; Verhoeven, J. W. *J. Phys. Chem. A* **1997**, *101*, 4867–4871.
(59) Hapiot, P.; Lagrost, C.; Le Floch, F.; Raoult, E.; Rault-Berthelot, J. *Chem. Mater.* **2005**, *17*, 2003–2012.
(60) Kay, C. W. M.; Elger, G.; Mobius, K. *Phys. Chem. Chem. Phys.* **1999**, *1*, 3999–4002.
(61) Dance, Z. E. X.; Mi, Q. X.; McCamant, D. W.; Ahrens, M. J.; Ratner, M. A.; Wasielewski, M. R. *J. Phys. Chem. B* **2006**, *110*, 25163–25173.
(62) Wasserman, E.; Snyder, L. C.; Yager, W. A. *J. Chem. Phys.* **1964**, *41*, 1763–1772.
(63) Gonen, O.; Levanon, H. *J. Phys. Chem.* **1984**, *88*, 4223–4228.
(64) van der Waals, J. H.; de Groot, M. S. In *The Triplet State*; Zahlan, A. B., Ed.; University Press: Cambridge, U.K., 1967; pp 101−132.
(65) El-Sayed, M. A. *Excited States* **1974**, *1*, 35–77.
(66) Siegel, S.; Judeikis, H. S. *J. Phys. Chem.* **1966**, *70*, 2201–2204.
(67) Thurnauer, M. C.; Norris, J. R. *Chem. Phys. Lett.* **1977**, *47*, 100–105.
(68) Okada, T.; Fujita, T.; Kubota, M.; Masaki, S.; Mataga, N.; Ide, R.; Sakata, Y.; Misumi, S. *Chem. Phys. Lett.* **1972**, *14*, 563–568.
(69) Wasielewski, M. R.; Johnson, D. G.; Svec, W. A.; Kersey, K. M.; Minsek, D. W. *J. Am. Chem. Soc.* **1988**, *110*, 7219–7221.
(70) Gaines, G. L., III; O'Neil, M. P.; Svec, W. A.; Niemczyk, M. P.; Wasielewski, M. R. *J. Am. Chem. Soc.* **1991**, *113*, 719–721.
(71) Kelley, R. F.; Shin, W. S.; Rybtchinski, B.; Sinks, L. E.; Wasielewski, M. R. *J. Am. Chem. Soc.* **2007**, *129*, 3173–3181.
(72) Yamauchi, S. *Bull. Chem. Soc. Jpn.* **2004**, *77*, 1255–1268.
(73) Yamauchi, S.; Takahashi, A.; Iwasaki, Y.; Unno, M.; Ohba, Y.; Higuchi, J.; Blank, A.; Levanon, H. *J. Phys. Chem. A* **2003**, *107*, 1478–1485.
(74) Weissman, S. I. *Acc. Chem. Res.* **1973**, *6*, 233–238.
(75) Lopez Ruperez, F.; Conesa, J. C.; Soria, J. *Spectrochim. Acta, Part A* **1984**, *40A*, 1021–1024.
(76) Till, U.; Hore, P. J. *Mol. Phys.* **1997**, *90*, 289–296.
(77) Fukuju, T.; Yashiro, H.; Maeda, K.; Murai, H.; Azumi, T. *J. Phys. Chem. A* **1997**, *101*, 7783–7786.
(78) Kobori, Y.; Shibano, Y.; Endo, T.; Tsuji, H.; Murai, H.; Tamao, K. *J. Am. Chem. Soc.* **2009**, *131*, 1624–1625.
(79) Davis, W. B.; Ratner, M. A.; Wasielewski, M. R. *J. Am. Chem. Soc.* **2001**, *123*, 7877–7886.
(80) Scott, A. M.; Miura, T.; Ricks, A. B.; Dance, Z. E. X.; Giacobbe, E. M.; Colvin, M. T.; Wasielewski, M. R. *J. Am. Chem. Soc.* **2009**, *131*, 17655–17666.

JP101523N